Hindawi
Complexity
Volume 2021, Article ID 6245168, 11 pages
https://doi.org/10.1155/2021/6245168

Research Article

Pursuer Navigation Based on Proportional Navigation and Optimal Information Fusion

Shulin Feng,[1] **Zhanxin Li**,[2] **Li Liu**,[1] **Hongyong Yang**,[1] **Yuanhua Yang**,[3] **Gaohuan Lv**,[4] **and Liang Yang**[1]

[1]*School of Information and Electrical Engineering, Ludong University, Yantai 264025, China*
[2]*Tianjin Key Laboratory of Microgravity and Hypogravity Environment Simulation Technology, Tianjin 300000, China*
[3]*School of Mathematics and Statistics Science, Ludong University, Yantai 264025, China*
[4]*Ulsan Ship and Ocean College, Ludong University, Yantai 264025, China*

Correspondence should be addressed to Shulin Feng; fengshulin@ldu.edu.cn

Received 19 May 2021; Accepted 13 September 2021; Published 21 October 2021

Academic Editor: Wen Qi

Pursuer navigation is proposed based on the three-dimensional proportional navigation law, and this method presents a family of navigation laws resulting in a rich behavior for different parameters. Firstly, the kinematics model for the pursuer and the target is established. Secondly, the proportional navigation law is deduced through the kinematics model. Based on point-to-point navigation, obstacle avoidance is implemented by adjusting the control parameters, and the combination can enrich the application range of obstacle avoidance and guidance laws. Thirdly, information fusion weighted by diagonal matrices is used for decreasing the tracking precision. Finally, simulations are conducted in the MATLAB environment. Simulation results verify the availability of the proposed navigation law.

1. Introduction

tVarious navigation and obstacle avoidance methods are the important issues. The proportional navigation is a method well known and widely applied in the aerospace community. In [1], the augmented IPN is deduced for interception. In [2], the authors present a new homing guidance law using well-known BPN to perform an impact time constraint and impact angle constraint. Over and above the case of infinite maneuverability of the missile, the full condition that captures a nonmaneuvering target is deduced in [3]. Real-time navigation is given in [4] by integrating the backstepping method and neurodynamics model. In [5], the proportional navigation applied to missile guidance problems is tailored. In [6], the authors propose collision avoidance strategy for multiagent. A receding horizon control method for convergent navigation of the robot is given in [7], and this method includes a scientific procedure for the generation of potential control sequences. In [8], a modified cooperative proportional navigation is presented to avoid singularity, and the time-to-go control efficiency under the small leading angle is improved in this paper. The capturability of 3D PPN against the lower speed freely-maneuvering target for the homing phase is restudied in [9], extending the NOR method of the 2D PPN to 3D space. In the study of [10], pure proportional navigation (PPN) and a look angle-constrained guidance law consisting of PPN and look angle control are designed. In [11], a novel augmented proportional navigation (APN) is proposed for midrange autonomous rendezvous, and the midrange autonomous rendezvous can be absolutely implemented. The application of proportional navigation to the pursuer requires improvements. The presentation of this paper is different from the classical presentation. The proportional navigation is proposed by using the flight path and heading angles of the pursuer. This presentation is more proper for the pursuer than the classical presentation, where proportional navigation is proposed in accordance with the lateral and vertical acceleration. Then, the presentation of proportional navigation can be easily adapted to the collision avoidance mode since the

proportional navigation is written as a function of the flight path and heading angles of the pursuer. It allows a rapid change in the path of the pursuer under proportional navigation.

In the study of [12], obstacle avoidance and navigation are addressed by using the model-based control method. This method can be used for both online and offline. In [12], the proportional navigation is written based on the robotic steering angle. Moreover, the collision avoidance mode is implemented by using proportional navigation. Notwithstanding the method of [12] seems to be quite competent, and it sustains the following problems.

(1) The control law for the orientation angle can continue to be expanded

(2) The proportional navigation was proposed by assuming no sensor noise

(3) Information fusion is not combined with the proportional navigation to improve the tracking process

In this paper, the work is mainly motivated by the study in [12]. The aim of this paper is to consider the solution of the pursuer tracking toward a target in the 3D space. Based on the geometric relationship of pursuer-target, this paper presents the polar kinematics models. In this paper, the proportional navigation is given in terms of the flight path and heading angles for the pursuer. Moreover, the proportional navigation can also be adapted to the collision avoidance mode. The method can be used for indoor and outdoor navigation as well, especially to reach goals that are at a long distance from the pursuer, and as a result, they are out of the range of view of the sensors (such as the camera), but their position is known to the pursuer.

The proportional navigation of Belkhouche and Belkhouche [12] was proposed by assuming no sensor noise. For sensor noise, the filter method can be used to improve the tracking process. As studied in [13], a data-driven method combining the EKF and RBF neural network is given to estimate the internal temperature for the lithium-ion battery. In [14], the particle filter is applied to predict the aging trajectory of the lithium-ion battery. Even though the algorithm of Belkhouche and Belkhouche [12] seems to be quite efficient, it suffers from that Kalman filter techniques are not used for dynamic state estimation. Various multisensor fusion methods have been studied to solve this problem. Under the optimal fusion criterion of Sun and Deng [15], the multisensor fusion decentralized Kalman filter is obtained. In [16], the authors propose the two-sensor information fusion steady-state Kalman filter. In [17, 18], distributed optimal information fusion filter theory is presented under the classical Kalman filter. The device are argued in [19] in accordance with sensor data fusion methods, sensor design, and prototype setup. Based on multisensor fusion, a hybrid indoor localization system is given in [20]. In [21], the authors present the information fusion Kalman filter weighted by scalars. In [22], the functional equivalence of two optimal measurement fusion methods is proved under the steady-state Kalman filter. Information fusion weighted by diagonal matrices is proposed in [16–18]. As studied in [12], this method is not considered the negative influence of sensor noise. Based on the above control theory of information fusion, the control strategy of [12] can be further improved. In this paper, the proportional navigation combined with information fusion weighted by diagonal matrices are used to implement more reasonable tracking performance.

Control objective of this paper is to implement pursuer navigation and obstacle avoidance using a easy and valid model-based control law. It can be applied to both online and offline navigation and obstacle avoidance. This method consists of a family of methods for pursuer navigation under proportional navigation, where this paper applies the pursuer kinematics equations combined with the geometric rule. The challenge of this paper is how to design the control law for proportional navigation and implement obstacle avoidance. To deal with the challenge, this paper presents the polar kinematics models of pursuer-target. The control law of proportional navigation is given in terms of the flight path and heading angles for the pursuer. Under sensor noise, two-sensor information fusion is applied to improve the control law. Moreover, the proportional navigation can implement collision avoidance by using point-to-point navigation.

The contribution of this paper is mainly to present three-dimensional proportional navigation to implement tracking the target, outperforming the pure proportional navigation (PPN) in terms of interception time. Under sensor noise, two-sensor information fusion together with proportional navigation can enhance the tracking precision. Moreover, obstacle avoidance is implemented by using point-to-point navigation combined with proportional navigation.

The remainder of this paper is organized as follows. The dynamic model of pursuer-target is derived. Then, the proportional navigation law is discussed. This paper designs the control method of obstacle avoidance. Two-sensor information fusion is used in this paper. Simulation results are given to formulate the availability of the obtained results, and then, some conclusions are drawn.

2. Dynamic Model

The geometry of the navigation is illustrated in Figure 1. In the 3D coordinate system, the linear velocity of the pursuer is v_P. The flight path and heading angles are θ_P and ϕ_P, respectively. LOS for target-pursuer is TP. σ_{TP} is the pitch angle of TP, and γ_{TP} is the yaw angle of TP. r_{TP} is the relative distance pursuer-target.

Based on [23, 24], the differential equations for r_{TP}, σ_{TP}, and γ_{TP} are

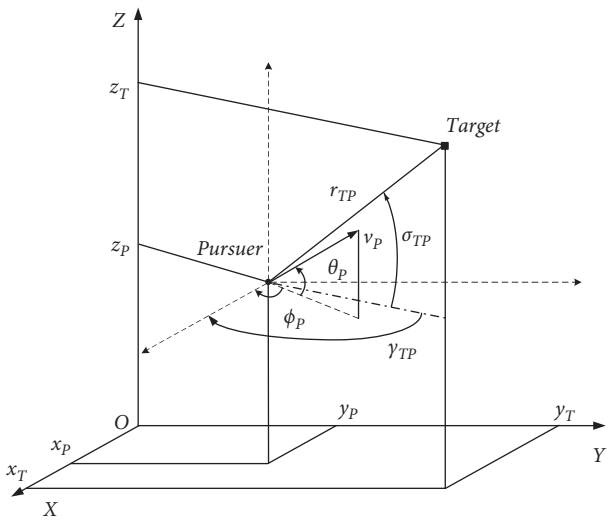

Figure 1: Geometric relationship of pursuer-target.

$$\begin{cases} \dot{r}_{\mathrm{TP}} = -v_P \cos(\sigma_{\mathrm{TP}} - \theta_P)\cos(\gamma_{\mathrm{TP}} - \phi_P) + v_T \cos(\sigma_{\mathrm{TP}} - \theta_T)\cos(\gamma_{\mathrm{TP}} - \phi_T), \\ r_{\mathrm{TP}}\dot{\sigma}_{\mathrm{TP}} = v_P \sin(\sigma_{\mathrm{TP}} - \theta_P)\cos(\gamma_{\mathrm{TP}} - \phi_P) - v_T \sin(\sigma_{\mathrm{TP}} - \theta_T)\cos(\gamma_{\mathrm{TP}} - \phi_T), \\ r_{\mathrm{TP}} \cos\ \sigma_{\mathrm{TP}}\dot{\gamma}_{\mathrm{TP}} = v_P \cos\ \theta_P \sin(\gamma_{\mathrm{TP}} - \phi_P) - v_T \cos\ \theta_T \sin(\gamma_{\mathrm{TP}} - \phi_T). \end{cases} \tag{1}$$

Since the target is motionless, one can have $v_T = 0$, and thus,

$$\begin{cases} \dot{r}_{\mathrm{TP}} = -v_P \cos(\sigma_{\mathrm{TP}} - \theta_P)\cos(\gamma_{\mathrm{TP}} - \phi_P), \\ r_{\mathrm{TP}}\dot{\sigma}_{\mathrm{TP}} = v_P \sin(\sigma_{\mathrm{TP}} - \theta_P)\cos(\gamma_{\mathrm{TP}} - \phi_P), \\ r_{\mathrm{TP}} \cos\ \sigma_{\mathrm{TP}}\dot{\gamma}_{\mathrm{TP}} = v_P \cos\ \theta_P \sin(\gamma_{\mathrm{TP}} - \phi_P). \end{cases} \tag{2}$$

The robustness of the method is a critical issue. It is should be noted that this method belongs to a family of methods in terms of the kinematics equation and geometric rule. These methods are famous for the robustness.

3. Three-Dimensional Proportional Navigation Law

This paper designs the proportional navigation law in conformity to the pursuer flight path and heading angles as follows:

$$\begin{cases} \theta_P(t) = G\sigma_{\mathrm{TP}}(t) + \delta, \\ \phi_P(t) = E\gamma_{\mathrm{TP}}(t) + \mu, \end{cases} \tag{3}$$

where G and E are the navigation constant with $(G \geq 1;\ E \geq 1)$ and δ and μ are the deviation angles.

Combining equation (2) with equation (3), the differential equations for r_{TP}, σ_{TP}, and γ_{TP} are

$$\begin{cases} \dot{r}_{\mathrm{TP}} = -v_P \cos[(G-1)\sigma_{\mathrm{TP}} + \delta]\cos((E-1)\gamma_{\mathrm{TP}} + \mu), \\ r_{\mathrm{TP}}\dot{\sigma}_{\mathrm{TP}} = -v_P \sin((G-1)\sigma_{\mathrm{TP}} + \delta)\cos[(E-1)\gamma_{\mathrm{TP}} + \mu], \\ r_{\mathrm{TP}} \cos\ \sigma_{\mathrm{TP}}\dot{\gamma}_{\mathrm{TP}} = -v_P \cos\ \theta_P \sin[(E-1)\gamma_{\mathrm{TP}} + \mu]. \end{cases} \tag{4}$$

Results in relation to the pursuer that tracks an immovable point are given as follows.

Theory 1. By using pure pursuit with $(G = E = 1;\ \delta = \mu = 0)$, the pursuer can reach the target from any original condition.

Proof. Combining $(G = E = 1,\ \delta = \mu = 0)$ with equation (4), it can be written as

$$\dot{r}_{\mathrm{TP}} = -v_P. \tag{5}$$

Since $\dot{r}_{\mathrm{TP}} < 0$, r_{TP} is decreasing and the pursuer can reach the target, with the final flight path angle $\theta_P(t_f) = \sigma_{\mathrm{TP}}(t_0)$ and heading angle $\phi_P(t_f) = \gamma_{\mathrm{TP}}(t_0)$.

This completes the proof. □

Theory 2. By using deviated pursuit with $(G = E = 1, \delta \neq 0, \text{and } \mu \neq 0)$, the pursuer can reach the target when

$$\delta, \mu \in \left[-\frac{\pi}{2}, \frac{\pi}{2}\right] \text{ or } \delta, \mu \in \left[\frac{\pi}{2}, \frac{3\pi}{2}\right]. \tag{6}$$

Proof. On the basis of the first equation in the relative kinematics model, one can obtain

$$\dot{r}_{\mathrm{TP}} = -v_P \cos\,\delta\,\cos\,\mu. \tag{7}$$

$\dot{r}_{\mathrm{TP}}$ is a decreasing function when δ and $\mu \in [-\pi/2, \pi/2]$ or δ and $\mu \in [\pi/2, 3\pi/2]$.

This completes the proof. □

Theory 3. For $G > 1$ and $E > 1$, the pursuer navigating under equation (3) reaches the target for nearly all original states.

Proof. Combining $(G > 1; E > 1)$ with equation (4), it obtains

$$\begin{cases} \dot{\sigma}_{\mathrm{TP}} = -\dfrac{v_P}{r_{\mathrm{TP}}}\sin\left[(G-1)\sigma_{\mathrm{TP}} + \delta\right]\cos\left[(E-1)\gamma_{\mathrm{TP}} + \mu\right] = f_{\mathrm{TP}}\left(\sigma_{\mathrm{TP}}, \gamma_{\mathrm{TP}}\right), \\ \dot{\gamma}_{\mathrm{TP}} = -\dfrac{v_P}{r_{\mathrm{TP}}}\dfrac{\cos\left(G\sigma_{\mathrm{TP}} + \delta\right)}{\cos\,\sigma_{\mathrm{TP}}}\sin\left[(E-1)\gamma_{\mathrm{TP}} + \mu\right] = g_{\mathrm{TP}}\left(\sigma_{\mathrm{TP}}, \gamma_{\mathrm{TP}}\right). \end{cases} \tag{8}$$

This system has four equilibrium solutions, namely, $(\sigma^*_{\mathrm{TP}_1} = 2n\pi - \delta/G - 1, \gamma^*_{\mathrm{TP}_1} = 2n\pi - \mu/E - 1)$, $(\sigma^*_{\mathrm{TP}_2} = 2n\pi - \delta/G - 1, \gamma^*_{\mathrm{TP}_2} = 2n\pi + \pi - \mu/E - 1)$, $(\sigma^*_{\mathrm{TP}_3} = 2n\pi + \pi - \delta/G - 1, \gamma^*_{\mathrm{TP}_3} = 2n\pi - \mu/E - 1)$, and $(\sigma^*_{\mathrm{TP}_4} = 2n\pi + \pi - \delta/G - 1, \gamma^*_{\mathrm{TP}_4} = 2n\pi + \pi - \mu/E - 1)$.

After partial deviation, it can be obtained that

$$\begin{aligned} \frac{\partial f_{\mathrm{TP}}}{\partial \sigma_{\mathrm{TP}}} &= -\frac{v_P}{r_{\mathrm{TP}}}(G-1)\cos\left[(G-1)\sigma_{\mathrm{TP}} + \delta\right]\cos\left[(E-1)\gamma_{\mathrm{TP}} + \mu\right], \\ \frac{\partial f_{\mathrm{TP}}}{\partial \gamma_{\mathrm{TP}}} &= \frac{v_P}{r_{\mathrm{TP}}}(E-1)\sin\left[(G-1)\sigma_{\mathrm{TP}} + \delta\right]\sin\left[(E-1)\gamma_{\mathrm{TP}} + \mu\right], \\ \frac{\partial g_{\mathrm{TP}}}{\partial \sigma_{\mathrm{TP}}} &= \frac{v_P}{r_{\mathrm{TP}}}\sin\left[(E-1)\gamma_{\mathrm{TP}} + \mu\right]\frac{(G-1)\sin\left(G\sigma_{\mathrm{TP}} + \delta\right)\cos\,\sigma_{\mathrm{TP}} + \sin\left[(G-1)\sigma_{\mathrm{TP}} + \delta\right]}{\cos^2\sigma_{\mathrm{TP}}}, \\ \frac{\partial g_{\mathrm{TP}}}{\partial \gamma_{\mathrm{TP}}} &= -\frac{v_P}{r_{\mathrm{TP}}}(E-1)\cos\left[(E-1)\gamma_{\mathrm{TP}} + \mu\right]\frac{\cos\left(G\sigma_{\mathrm{TP}} + \delta\right)}{\cos\,\sigma_{\mathrm{TP}}} \\ &= -\frac{(E-1)v_P}{r_{\mathrm{TP}}}\cos\left[(E-1)\gamma_{\mathrm{TP}} + \mu\right]\frac{\cos\left[(G+1)\sigma_{\mathrm{TP}} + \delta\right] + \cos\left[(G-1)\sigma_{\mathrm{TP}} + \delta\right]}{2\,\cos^2\sigma_{\mathrm{TP}}}. \end{aligned} \tag{9}$$

By linearizing near each equilibrium solution, one has

$$
\begin{aligned}
T_1 &= \begin{bmatrix} \dfrac{\partial f_{\mathrm{TP}}}{\partial \sigma_{\mathrm{TP}}}\Big|_{\left(\sigma^*_{\mathrm{TP}_1},\gamma^*_{\mathrm{TP}_1}\right)} & \dfrac{\partial f_{\mathrm{TP}}}{\partial \gamma_{\mathrm{TP}}}\Big|_{\left(\sigma^*_{\mathrm{TP}_1},\gamma^*_{\mathrm{TP}_1}\right)} \\ \dfrac{\partial g_{\mathrm{TP}}}{\partial \sigma_{\mathrm{TP}}}\Big|_{\left(\sigma^*_{\mathrm{TP}_1},\gamma^*_{\mathrm{TP}_1}\right)} & \dfrac{\partial g_{\mathrm{TP}}}{\partial \gamma_{\mathrm{TP}}}\Big|_{\left(\sigma^*_{\mathrm{TP}_1},\gamma^*_{\mathrm{TP}_1}\right)} \end{bmatrix} \\
&= \begin{bmatrix} -\dfrac{(G-1)v_P}{r_{\mathrm{TP}}} & 0 \\ 0 & -\dfrac{(E-1)v_P}{2r_{\mathrm{TP}}}\dfrac{\cos\left[(G+1)\sigma_{\mathrm{TP}}+\delta\right]+1}{\cos^2\sigma_{\mathrm{TP}}} \end{bmatrix} = \begin{pmatrix} \lambda_{11} & 0 \\ 0 & \lambda_{12} \end{pmatrix}, \\
T_2 &= \begin{bmatrix} \dfrac{\partial f_{\mathrm{TP}}}{\partial \sigma_{\mathrm{TP}}}\Big|_{\left(\sigma^*_{\mathrm{TP}_2},\gamma^*_{\mathrm{TP}_2}\right)} & \dfrac{\partial f_{\mathrm{TP}}}{\partial \gamma_{\mathrm{TP}}}\Big|_{\left(\sigma^*_{\mathrm{TP}_2},\gamma^*_{\mathrm{TP}_2}\right)} \\ \dfrac{\partial g_{\mathrm{TP}}}{\partial \sigma_{\mathrm{TP}}}\Big|_{\left(\sigma^*_{\mathrm{TP}_2},\gamma^*_{\mathrm{TP}_2}\right)} & \dfrac{\partial g_{\mathrm{TP}}}{\partial \gamma_{\mathrm{TP}}}\Big|_{\left(\sigma^*_{\mathrm{TP}_2},\gamma^*_{\mathrm{TP}_2}\right)} \end{bmatrix} \\
&= \begin{pmatrix} \dfrac{(G-1)v_P}{r_{\mathrm{TP}}} & 0 \\ 0 & -\dfrac{(E-1)v_P}{2r_{\mathrm{TP}}}\dfrac{\cos\left[(G+1)\sigma_{\mathrm{TP}}+\delta\right]-1}{\cos^2\sigma_{\mathrm{TP}}} \end{pmatrix} = \begin{pmatrix} \lambda_{21} & 0 \\ 0 & \lambda_{22} \end{pmatrix}, \\
T_3 &= \begin{bmatrix} \dfrac{\partial f_{\mathrm{TP}}}{\partial \sigma_{\mathrm{TP}}}\Big|_{\left(\sigma^*_{\mathrm{TP}_3},\gamma^*_{\mathrm{TP}_3}\right)} & \dfrac{\partial f_{\mathrm{TP}}}{\partial \gamma_{\mathrm{TP}}}\Big|_{\left(\sigma^*_{\mathrm{TP}_3},\gamma^*_{\mathrm{TP}_3}\right)} \\ \dfrac{\partial g_{\mathrm{TP}}}{\partial \sigma_{\mathrm{TP}}}\Big|_{\left(\sigma^*_{\mathrm{TP}_3},\gamma^*_{\mathrm{TP}_3}\right)} & \dfrac{\partial g_{\mathrm{TP}}}{\partial \gamma_{\mathrm{TP}}}\Big|_{\left(\sigma^*_{\mathrm{TP}_3},\gamma^*_{\mathrm{TP}_3}\right)} \end{bmatrix} \\
&= \begin{pmatrix} \dfrac{(G-1)v_P}{r_{\mathrm{TP}}} & 0 \\ 0 & a-\dfrac{(E-1)v_P}{2r_{\mathrm{TP}}}\dfrac{\cos\left[(G+1)\sigma_{\mathrm{TP}}+\delta\right]+1}{\cos^2\sigma_{\mathrm{TP}}} \end{pmatrix} = \begin{pmatrix} \lambda_{31} & 0 \\ 0 & \lambda_{32} \end{pmatrix}, \\
T_4 &= \begin{bmatrix} \dfrac{\partial f_{\mathrm{TP}}}{\partial \sigma_{\mathrm{TP}}}\Big|_{\left(\sigma^*_{\mathrm{TP}_4},\gamma^*_{\mathrm{TP}_4}\right)} & \dfrac{\partial f_{\mathrm{TP}}}{\partial \gamma_{\mathrm{TP}}}\Big|_{\left(\sigma^*_{\mathrm{TP}_4},\gamma^*_{\mathrm{TP}_4}\right)} \\ \dfrac{\partial g_{\mathrm{TP}}}{\partial \sigma_{\mathrm{TP}}}\Big|_{\left(\sigma^*_{\mathrm{TP}_4},\gamma^*_{\mathrm{TP}_4}\right)} & \dfrac{\partial g_{\mathrm{TP}}}{\partial \gamma_{\mathrm{TP}}}\Big|_{\left(\sigma^*_{\mathrm{TP}_4},\gamma^*_{\mathrm{TP}_4}\right)} \end{bmatrix} \\
&= \begin{pmatrix} -\dfrac{(G-1)v_P}{r_{\mathrm{TP}}} & 0 \\ 0 & -\dfrac{(E-1)v_P}{2r_{\mathrm{TP}}}\dfrac{\cos\left[(G+1)\sigma_{\mathrm{TP}}+\delta\right]-1}{\cos^2\sigma_{\mathrm{TP}}} \end{pmatrix} = \begin{pmatrix} \lambda_{41} & 0 \\ 0 & \lambda_{42} \end{pmatrix}.
\end{aligned} \tag{10}
$$

The characteristic roots λ_{11} and λ_{12} of T_1 are with ($\lambda_{11}<0$ and $\lambda_{12}<0$), the characteristic roots λ_{21} and λ_{22} of T_2 are with ($\lambda_{21}>0$ and $\lambda_{22}>0$), the characteristic roots λ_{31} and λ_{32} of T_3 are with ($\lambda_{31}>0$ and $\lambda_{32}<0$), the characteristic roots λ_{41} and λ_{42} of T_4 are with ($\lambda_{41}<0$ and $\lambda_{42}>0$). According to Hartman and Grobman theorem of [25, 26], only $(\sigma^*_{\mathrm{TP}_1},\gamma^*_{\mathrm{TP}_1})$ is asymptotically stable.

Since the solutions for σ_{TP} and γ_{TP} approach their asymptotically stable equilibrium positions, one can get $\sigma_{\mathrm{TP}} \longrightarrow \sigma^*_{\mathrm{TP}_1} = 2n\pi - \delta/G - 1$ and $\gamma_{\mathrm{TP}} \longrightarrow \gamma^*_{\mathrm{TP}_1} = 2n\pi - \mu/E - 1$ with time. Since $\sigma_{\mathrm{TP}} \longrightarrow 2n\pi - \delta/G - 1$ and $\gamma_{\mathrm{TP}} \longrightarrow 2n\pi - \mu/E - 1$ with time, $\cos[(G-1)\sigma_{\mathrm{TP}} + \delta]\cos[(E-1)\gamma_{\mathrm{TP}} + \mu]$ is positive in $[t_1, t_f]$, $t_1 \geq t_0$; then, one can get $\dot{r}_{\mathrm{TP}} < 0$ after t_1.

This completes the proof.

At t_0, the proportional navigation law is

$$\left\{ \theta_P(t_0) = G\sigma_{\mathrm{TP}}(t_0) + \delta\phi_P(t_0) = E\gamma_{\mathrm{TP}}(t_0) + \mu. \right. \tag{11}$$

Then, two cases are

(i) Select (G, E) and (δ, μ) according to equation (11) on (G and $E \geq 1$).

(ii) Put into use heading regulation which deduces θ_P and ϕ_P from their original values to the values which satisfy equation (11) for (G, E) and (δ, μ). This method which gives more adaptability for the selection of (G, E) and (δ, μ). □

4. Obstacle Avoidance

For simplicity and without loss of generality, obstacles are denoted by spheres S_j. Spheres S_j has d as a radius.

Points E_1 and E_2 are shown in Figure 2. r_{j_1} and r_{j_2} are the distances from the pursuer to E_1 and E_2, respectively. The differential equations for r_{jk}, σ_{jk}, and γ_{jk} between the pursuer and the center of obstacle S_j are

$$\begin{cases} \dot{r}_{jk} = -v_P \cos\left(G\sigma_{\mathrm{TP}} + \delta - \sigma_{jk}\right)\cos\left(E\gamma_{\mathrm{TP}} + \mu - \gamma_{jk}\right), \\ r_{jk}\dot{\sigma}_{jk} = -v_P \sin\left(G\sigma_{\mathrm{TP}} + \delta - \sigma_{jk}\right)\cos\left(E\gamma_{\mathrm{TP}} + \mu - \gamma_{jk}\right), \\ r_{jk}\cos\,\sigma_{jk}\dot{\gamma}_{jk} = -v_P \cos\left(G\sigma_{\mathrm{TP}} + \delta\right)\sin\left(E\gamma_{\mathrm{TP}} + \mu - \gamma_{jk}\right). \end{cases} \tag{12}$$

With $k = 1$ and 2, one can identify whether the pursuer is oncoming or deviating from the obstacle based on equation (12). The pursuer is in a collision when

$$\left\{ \theta_P(t) \in \left[\sigma_{j_1}, \sigma_{j_2}\right]\phi_P(t) \in \left[\gamma_{j_1}, \gamma_{j_2}\right], \right. \tag{13}$$

where $\sigma_{j_1} < \sigma_{j_2}$ and $\gamma_{j_1} < \gamma_{j_2}$. The avoidance course of the proportional navigation is

$$\left\{ G\sigma_{\mathrm{TP}}(t) + \delta \notin \left[\sigma_{j_1}, \sigma_{j_2}\right] E\gamma_{\mathrm{TP}}(t) + \mu \notin \left[\gamma_{j_1}, \gamma_{j_2}\right], \right. \tag{14}$$

when the pursuer is within a definite distance d_0 from the obstacle.

This section can provide free or obstacle directions, which is designed in consideration of the obstacles as follows:

$$q_j = \begin{cases} 1, & \theta_P(t) \in \left[\sigma_{j_1}, \sigma_{j_2}\right] \phi_P(t) \in \left[\gamma_{j_1}, \gamma_{j_2}\right], \\ 0, & \text{otherwise.} \end{cases} \tag{15}$$

With $Q = \cup_{j=1}^{K} q_j$, where K is the total amount of obstacles.

Point T_1 corresponds to a free direction. T_0 is the point where the pursuer starts deviating from a possible obstacle. When $(r_i - d) < d_0$, the pursuer is driven to an intermediary target that occurs in a free direction.

$\sigma^0_{\mathrm{TP}_0}$ and $\gamma^0_{\mathrm{TP}_0}$ denote the pitch angle and yaw angle of pursuer-target measured at point T_0 at time t^0_1, and $\sigma^1_{\mathrm{TP}_0}$ and $\gamma^1_{\mathrm{TP}_0}$ the pitch angle and yaw angle pursuer-point T_1 measured at point T_0 at the same time. $(\sigma^0_{\mathrm{TP}_0}, \gamma^0_{\mathrm{TP}_0})$ and $(\sigma^1_{\mathrm{TP}_0}, \gamma^1_{\mathrm{TP}_0})$ are

$$\begin{cases} \tan\,\sigma^0_{\mathrm{TP}_0} = \dfrac{z_T - z_P\left(t^0_1\right)}{\sqrt{\left(x_T - x_P\left(t^0_1\right)\right)^2 + \left(y_T - y_P\left(t^0_1\right)\right)^2}} \tan\,\gamma^0_{\mathrm{TP}_0} = \dfrac{y_T - y_P\left(t^0_1\right)}{z_T - z_P\left(t^0_1\right)}, \\ \tan\,\sigma^1_{\mathrm{TP}_0} = \dfrac{z_{T_1} - z_P\left(t^0_1\right)}{\sqrt{\left(x_{T_1} - x_P\left(t^0_1\right)\right)^2 + \left(y_{T_1} - y_P\left(t^0_1\right)\right)^2}} \tan\,\gamma^1_{\mathrm{TP}_0} = \dfrac{y_{T_1} - y_P\left(t^0_1\right)}{z_{T_1} - z_P\left(t^0_1\right)}, \end{cases} \tag{16}$$

where $(x_{T_1}, y_{T_1}, z_{T_1})$ are the coordinates of point T_1. For the flatness of the path, then

$$\begin{cases} G_0\sigma^0_{\mathrm{TP0}} + \delta_0 = G_1\sigma^1_{\mathrm{TP0}} + \delta_1 \\ E_0\gamma^0_{\mathrm{TP0}} + \mu_0 = E_1\gamma^1_{\mathrm{TP0}} + \mu_1. \end{cases} \tag{17}$$

One can determine values of (G_1, δ_1) and (E_1, μ_1) that fulfill equation (17) and move the pursuer to point T_1. If the pursuer suffers other obstacles, this strategy is repeated.

5. Two-Sensor Information Fusion

Two-sensor discrete-time system is

$$\left\{ x(\tau + 1) = Bx(\tau) + w(\tau) y_i(\tau) = \Upsilon_i x(\tau) + v_i(\tau), \quad i = 1 \text{ and } 2, \right. \tag{18}$$

where

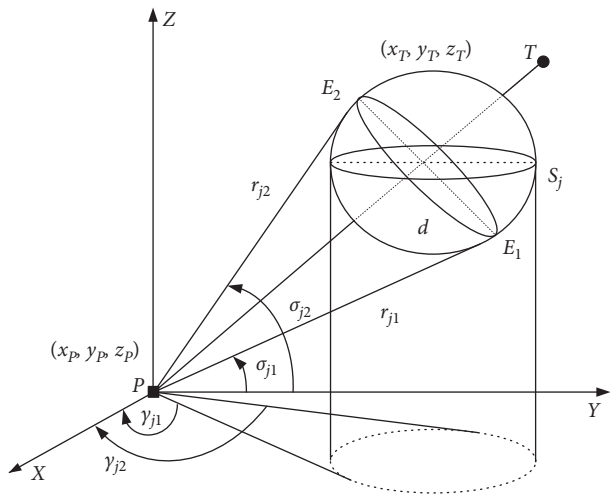

Figure 2: Representation of obstacle avoidance.

$$B = \begin{bmatrix} 1 & 0 & 0 \\ 0 & 1 & 0 \\ 0 & 0 & 1 \end{bmatrix}, \quad \Upsilon_i = \begin{bmatrix} 1 & 0 & 0 \\ 0 & 1 & 0 \\ 0 & 0 & 1 \end{bmatrix}. \tag{19}$$

Based on [27], the local optimal Kalman filter is

$$\begin{aligned} \widehat{x}_i(\tau|\tau) &= \left[I_n - K_i(\tau)\Upsilon_i\right]B\widehat{x}_i(\tau-1|\tau-1) + K_i(\tau)y_i(\tau), \\ K_i(\tau) &= P_i(\tau|\tau-1)\Upsilon_i^T\left[\Upsilon_i P_i(\tau|\tau-1)\Upsilon_i^T + R_i\right]^{-1}, \\ P_i(\tau|\tau-1) &= BP_i(\tau-1|\tau-1)B^T + \mathrm{GQG}^T, \\ P_i(\tau|\tau) &= \left[I_n - K_i(\tau)\Upsilon_i\right]P_i(\tau|\tau-1). \end{aligned} \tag{20}$$

Thus, the optimal Kalman filter is

$$\widehat{x}_0(\tau|\tau) = \zeta_1(\tau)\widehat{x}_1(\tau|\tau) + \zeta_2(\tau)\widehat{x}_2(\tau|\tau). \tag{21}$$

The optimal matrix of weight coefficients designed in [17, 18] can be calculated as

$$\zeta_i = \mathrm{diag}\left(\alpha_{i_1}, \alpha_{i_2}, \ldots, \alpha_{\mathrm{in}}\right), \quad i = 1 \text{ and } 2, \tag{22}$$

where the optimal weight coefficients are

$$\alpha_{1i} = \frac{P_2^{ii} - P_{12}^{ii}}{P_1^{ii} + P_2^{ii} - 2P_{12}^{ii}}, \quad \alpha_{2i} = \frac{P_1^{ii} - P_{12}^{ii}}{P_1^{ii} + P_2^{ii} - 2P_{12}^{ii}}, \tag{23}$$

where P_i^{ii} and P_{12}^{ii} are the diagonal element of P_i and P_{12}. The error covariance matrix is

$$P_{0i} = \frac{P_1^{ii}P_2^{ii} - \left(P_{12}^{ii}\right)^2}{P_1^{ii} + P_2^{ii} - 2P_{12}^{ii}}, i = 1, 2, \ldots, n. \tag{24}$$

The trace of the error covariance matrix for information fusion is

$$\mathrm{tr}P_0(\tau|\tau) = P_{01} + P_{02} + \cdots + P_{0n}, \tag{25}$$

where $\mathrm{tr}P_0 \le \mathrm{tr}P_i$, $i = 1$ and 2.

By using the Kalman estimator, fusion position of the target $(x_{T_{\mathrm{Fu}}}, y_{T_{\mathrm{Fu}}}, z_{T_{\mathrm{Fu}}})$ and the pursuer $(x_{P_{\mathrm{Fu}}}, y_{P_{\mathrm{Fu}}}, z_{P_{\mathrm{Fu}}})$ can be obtained. Thus, $\sigma_{\mathrm{Fu}} = \arctan z_{T_{\mathrm{Fu}}} - z_{P_{\mathrm{Fu}}} / \sqrt{\left(x_{T_{\mathrm{Fu}}} - x_{P_{\mathrm{Fu}}}\right)^2 + \left(y_{T_{\mathrm{Fu}}} - y_{P_{\mathrm{Fu}}}\right)^2}$ and $\gamma_{\mathrm{Fu}} = \arctan y_{T_{\mathrm{Fu}}} - y_{P_{\mathrm{Fu}}} / x_{T_{\mathrm{Fu}}} - x_{P_{\mathrm{Fu}}}$. Under two-sensor information fusion, equation (3) is written as

$$\begin{cases} \theta_{P_{\mathrm{Fu}}}(t) = G\sigma_{\mathrm{Fu}}(t) + \delta, \\ \phi_{P_{\mathrm{Fu}}}(t) = E\gamma_{\mathrm{Fu}}(t) + \mu. \end{cases} \tag{26}$$

6. Simulation Results

This section proposes several simulations, where tracking can be implemented under proportional navigation. In this section, distances velocities and time have been with units to achieve realistic results.

Example 1. The original position of air vehicle is (12 m, 12 m, 12 m), with $\theta_P(t_0) = \pi$ and $\phi_P(t_0) = \pi/2$. The aerial target is situated at (110 m, 110 m, 150.6 m); thus, $\sigma_{\mathrm{TP}}(t_0) = \pi/4$ and $\gamma_{\mathrm{TP}}(t_0) = \pi/4$. The solutions for the two approaches discussed above are as follows.

(1) Since $(\theta_P(t_0) = \pi, \phi_P(t_0) = \pi/2)$ and $(\sigma_{\mathrm{TP}}(t_0) = \pi/4, \gamma_{\mathrm{TP}}(t_0) = \pi/4)$, (G, δ) and (E, μ) are calculated such that

$$\begin{cases} \pi = G\dfrac{\pi}{4} + \delta, \\ \dfrac{\pi}{2} = E\dfrac{\pi}{4} + \mu. \end{cases} \tag{27}$$

There exists an infinite number of methods for (G, δ) and (E, μ) which satisfy equation (27), and hence, there exists an infinite number of possible trajectories for the air vehicle. One can take [$(G = 3, \delta =$

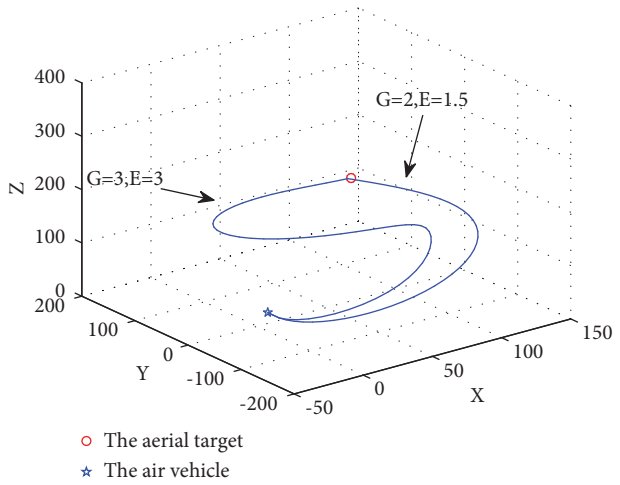

Figure 3: Configuration satisfied by selecting control parameters.

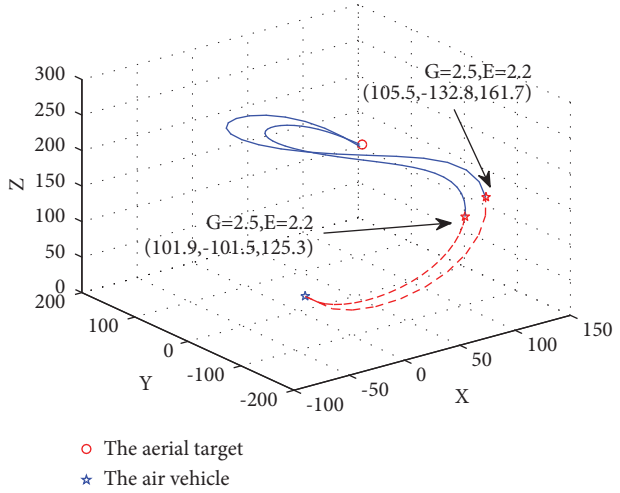

Figure 4: Illustration of the heading regulation.

$\pi/4)$, $(E = 3, \mu = -\pi/4)]$ or $[(G = 2, \delta = \pi/2), (E = 1.5, \mu = \pi/8)]$. Thus, the trajectory of the air vehicle is predefined by the original conditions and the values of (G, δ) and (E, μ). As illustrated in Figure 3, the air vehicle can reach the aerial target using this method.

(2) (G, δ) and (E, μ) are predetermined, and the heading regulation phase is necessary. Heading regulation is to take the air vehicle (θ_P^i, ϕ_P^i) from the initial values to the intermediary values $(\theta_{P_0}^i, \phi_{P_0}^i)$ that satisfy equation (11). One can take $(G = 2.5, \delta = 3\pi/8)$ and $(E = 2.2, \mu = -\pi/20)$.

There exist various potentialities for the selection of (x_P^i, y_P^i, z_P^i). One takes $(x_P^i, y_P^i, z_P^i) = (101.9\,\text{m}, -101.5\,\text{m}, 125.3\,\text{m})$; thus, $\theta_{P_0}^i = 1.61$ rad and $\phi_{P_0}^i = 3.2$ rad. One takes $(x_P^i, y_P^i, z_P^i) = (105.5\,\text{m}, -132.8\,\text{m}, 161.7\,\text{m})$; thus, $\theta_{P_0}^i = 1.33$ rad and $\phi_{P_0}^i = 3.26$ rad. Some methods from control theory are applied to the intention of heading regulation. The air vehicle navigation applying this method is shown in Figure 4. The dashed lines illustrate the path of the air vehicle under the heading regulation phase. This method can give more adaptability for the selection of (G, δ) and (E, μ).

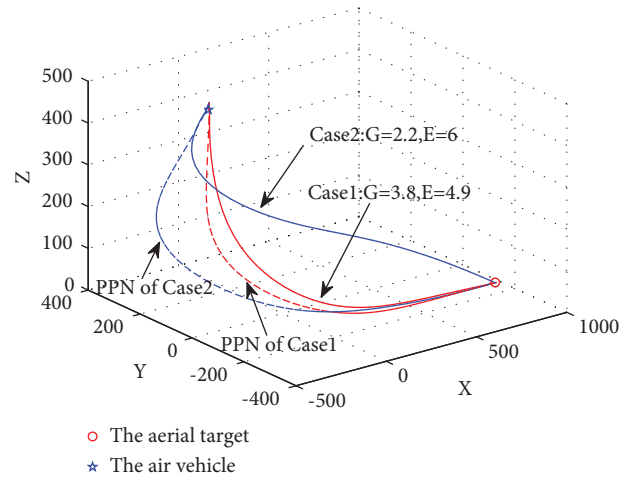

Figure 5: Comparison with proportional navigation and PPN.

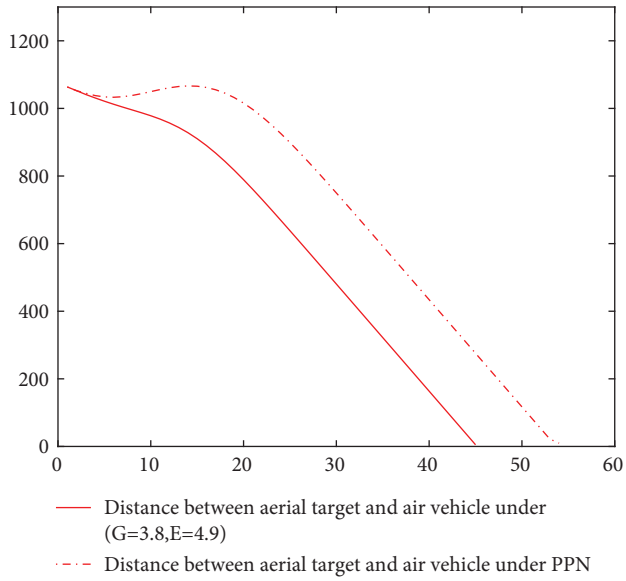

Figure 6: Distance between the aerial target and air vehicle under case 1.

Example 2. Comparison with the PPN, and this example will be considered. The original position of the air vehicle is (22 m, 300 m, 400 m), and the aerial target is situated at (880 m, −208 m, 30 m). In the first case, one can take $(G = 3.8, E = 4.9)$. From Figures 5 and 6, it is observed that the air vehicle navigating under proportional navigation reaches the aerial target before the PPN. The interception times are 45 s and 54 s for proportional navigation and PPN, respectively. In the second case, one can take $(G = 2.2, E = 6)$. From Figures 5 and 7, the interception times are 50 s and 63 s for proportional navigation and PPN, respectively. This example indicates that proportional

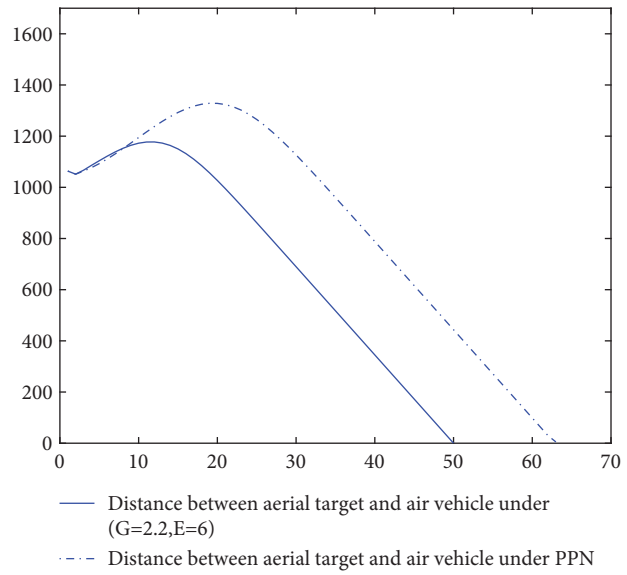

Figure 7: Distance between aerial target and air vehicle under case 2.

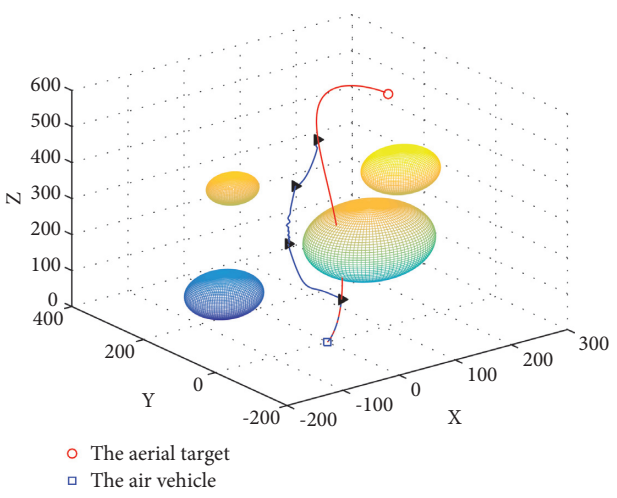

Figure 8: Online deviation at the appearance of spherical obstacles.

navigation can implement tracking the target, outperforming PPN in the field of interception time.

Example 3. At the appearance of spherical obstacles in a complicated environment, the point-to-point navigation method is applied to reach the aerial target and avoid the obstacles. The pursuer initiates from the initial position (0 m, 0 m, 0 m) and aims to reach the aerial target situated at (300 m, 300 m, 424.2 m). As illustrated in Figure 8, online deviation towards intermediary aerial targets T_1, T_2, T_3, and T_4 is applied with the following different control parameters. Phase PT_1: $(G = 2, \delta = \pi/4)$ and $(E = 1.2, \mu = 3\pi/40)$. Phase T_1T_2: $(G = 2.1, \delta = -10\pi/34)$ and $(E = 6.8, \mu = 10\pi/21)$. Phase T_2T_3: $(G = 2.1, \delta = -\pi/4)$ and $(E = 4, \mu = \pi/3)$. Phase T_3T_4: $(G = 1.3, \delta = -\pi/4)$ and $(E = 2, \mu = \pi/2)$. Phase T_4T: $(G = 2, \delta = \pi/4)$ and $(E = 1.2, \mu = 3\pi/40)$. The path of the air vehicle is $P \longrightarrow T_1 \longrightarrow T_2 \longrightarrow T_3 \longrightarrow T_4 \longrightarrow T$. These

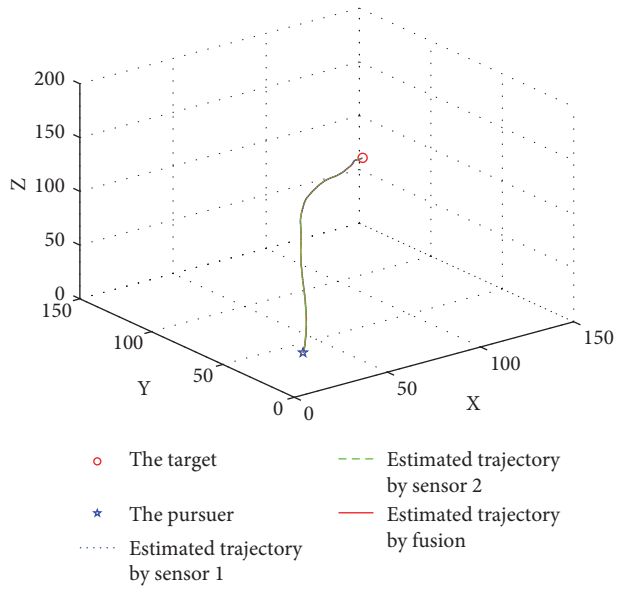

Figure 9: Filtered trajectory under proportional navigation.

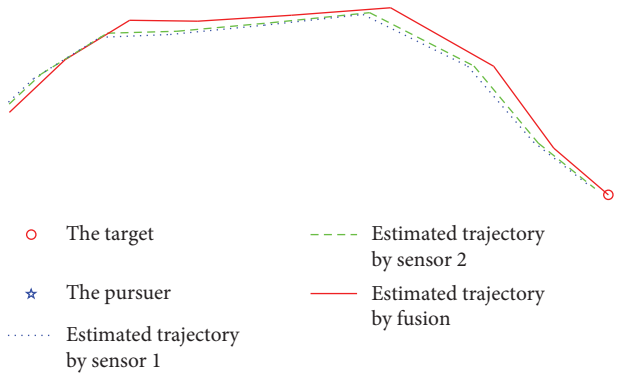

Figure 10: Enlargement in tracking result of Figure 9.

points can be selected so that the differences from the titular trajectory are small, which keeps smoothness of the trajectory. The air vehicle applies the point-to-point method to navigate towards the aerial target and avoid the obstacles.

Example 4. Under sensor noise, the initial position of the purser is (20 m, 20 m, 20 m) and the target is situated at (90 m, 90 m, 118.98 m). Thus, one can take $(G = 2, \delta = \pi/8)$ and $(E = 2, \mu = -\pi/8)$. In this case, two-sensor information fusion weighted by diagonal matrices together with proportional navigation is given to enhance the tracking precision. Figure 9 shows the filtered trajectory under proportional navigation. Enlargement in tracking result of Figure 9 is shown in Figure 10. The analysis of tracking performance indicates that the more higher the precision, the less the trace of the error covariance matrix. From Figure 11, one obtains $\mathrm{tr}P_i(k|k) > \mathrm{tr}P_0(k|k)$. As a result, the trace of error the covariance matrix under information fusion is lower than the value of the single sensor. Then, two-sensor information fusion provides proportional navigation with more accurate target estimates. This example shows

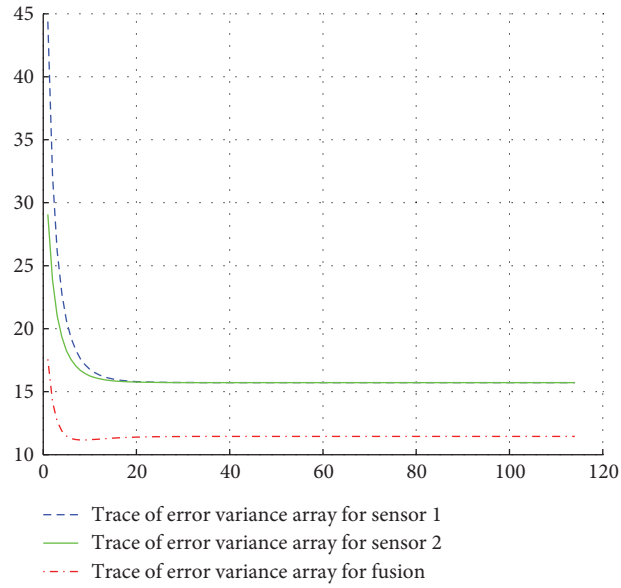

Figure 11: Trace of the error covariance matrix under two-sensor information fusion.

that the fusion result is better than that of the single sensor and the fusion method is effective.

7. Conclusion

This paper proposes a method for pursuer navigation under proportional navigation. The control strategy is primitive and depends on only the position of the target. For obstacle avoidance, this paper can avoid it by adjusting the control parameters. In the presence of sensor noise, the proportional navigation combined with information fusion weighted by diagonal matrices can achieve more reasonable interception performance. The method opens new directions for research, such as navigation using the proportional navigation under kinematics of pursuer and dynamics constraints and the influence of the control parameters, especially G and E.

Data Availability

The data used to support the findings of this study are available from the corresponding author upon request.

Conflicts of Interest

The authors declare that there are no conflicts of interest.

Acknowledgments

This work was supported by Key Laboratory of Cyber-Physical System and Intelligent Control in Universities of Shandong, Ph.D. Programs Foundation of Ludong University, National Natural Science Foundation of China (no. 61903172), and Open Project Program of Tianjin Key Laboratory of Microgravity and Hypogravity Environment Simulation Technology (no. TJWDZL2019KT003).

References

[1] N. Cho and Y. Kim, "Optimality of augmented ideal proportional navigation for maneuvering target interception," *IEEE Transactions on Aerospace and Electronic Systems*, vol. 52, no. 2, pp. 948–954, 2016.

[2] I. S. Jeon, J. I. Lee, and M. J. Tahk, "Impact-time-control guidance with generalized proportional navigation based on nonlinear formulation," *Journal of Guidance, Control, and Dynamics*, vol. 39, no. 8, pp. 1887–1892, 2016.

[3] F. Tyan, "Analysis of general ideal proportional navigation guidance laws," *Asian Journal of Control*, vol. 18, no. 3, pp. 899–919, 2016.

[4] S. X. Yang, A. Anmin Zhu, G. F. Guangfeng Yuan, and M. Q. Meng, "A bioinspired neurodynamics-based approach to tracking control of mobile robots," *IEEE Transactions on Industrial Electronics*, vol. 59, no. 8, pp. 3211–3220, 2012.

[5] S.-C. Han, H. Bang, and C.-S. Yoo, "Proportional navigation-based collision avoidance for UAVs," *International Journal of Control, Automation and Systems*, vol. 7, no. 4, pp. 553–565, 2009.

[6] P. Long, W. Liu, and J. Pan, "Deep-learned collision avoidance policy for distributed multiagent navigation," *IEEE Robotics and Automation Letters*, vol. 2, no. 2, pp. 656–663, 2017.

[7] M. Seder, M. Baotic, and I. Petrovic, "Receding horizon control for convergent navigation of a differential drive mobile robot," *IEEE Transactions on Control Systems Technology*, vol. 25, no. 2, pp. 653–660, 2017.

[8] Y. Chen, J. Wang, C. Wang, J. Shan, and M. Xin, "A modified cooperative proportional navigation guidance law," *Journal of the Franklin Institute*, vol. 356, no. 11, pp. 5692–5705, 2019.

[9] K. B. Li, H. S. Shin, A. Tsourdos, and M. Tahk, "Capturability of 3D PPN against lower-speed maneuvering target for homing phase," *IEEE Transactions on Aerospace and Electronic Systems*, vol. 56, no. 1, pp. 711–722, 2019.

[10] S. Lee, S. Ann, N. Cho, and Y. Kim, "Capturability of guidance laws for interception of nonmaneuvering target with field-of-view limit," *Journal of Guidance, Control, and Dynamics*, vol. 42, no. 4, pp. 869–884, 2019.

[11] Y. Liu, K. Li, L. Chen, and Y. Liang, "Novel augmented proportional navigation guidance law for mid-range autonomous rendezvous," *Acta Astronautica*, vol. 162, no. 9, pp. 526–535, 2019.

[12] F. Belkhouche and B. Belkhouche, "Wheeled mobile robot navigation using proportional navigation," *Advanced Robotics*, vol. 21, no. 3-4, pp. 395–420, 2007.

[13] K. Liu, K. Li, Q. Peng, Y. Guo, and L. Zhang, "Data-driven hybrid internal temperature estimation approach for battery thermal management," *Complexity*, vol. 2018, Article ID 9642892, 15 pages, 2018.

[14] X. Tang, K. Liu, X. Wang, B. Liu, F. Gao, and W. D. Widanage, "Real-time aging trajectory prediction using a base model-oriented gradient-correction particle filter for lithium-ion batteries," *Journal of Power Sources*, vol. 440, Article ID 227118, 2019.

[15] S.-L. Sun and Z.-L. Deng, "Multi-sensor optimal information fusion kalman filter," *Automatica*, vol. 40, no. 6, pp. 1017–1023, 2004.

[16] Y. Gao, L. Mao, Z. J. Liang, and Z. L. Deng, "Two-sensor information fusion steady-state kalman filter weighted by diagonal matrices," *Science Technology and Engineering*, vol. 21, no. 2, pp. 52–54, 2004.

[17] Z. L. Deng, *Optimal Estimation Theory with Applications*, Harbin Institute of Technology Press, Harbin, China, 2005.

[18] Z. L. Deng, *Information Fusion Filtering Theory with Applications*, Harbin Institute of Technology Press, Harbin, China, 2007.
[19] J. J. Gu, M. Meng, A. Cook, and G. Faulkner, "Simulation study of artificial ocular movement with intelligent control," *Control Engineering Practice*, vol. 13, no. 4, pp. 509–518, 2005.
[20] Y. L. Shi, W. M. Zhang, Z. Yao et al., "Design of a hybrid indoor location system based on multi-sensor fusion for robot navigation," *Sensors*, vol. 18, no. 10, pp. 1–18, 2018.
[21] S. L. Sun and P. Y. Cui, "Two sensors optimal information fusion kalman filter and its application in tracking systems," *Journal of Astronautics*, vol. 24, no. 2, pp. 206–209, 2003.
[22] Z. L. Deng, C. X. Cui, and J. G. Bai, "On functional equivalence of two measurement fusion methods based on steady-state kalman filtering," *Science Technology and Engineering*, vol. 4, no. 11, pp. 897–902, 2004.
[23] S. A. Elgamel and A. H. Makaryous, "Performance of modern guided systems in presence of jamming signal," in *Proceedings of the International Conference on Aerospace Science and Aviation Technology*, Cairo, Egypt, 2001.
[24] S. A. Elgamel and J. J. Soraghan, "Target tracking enhancement using a kalman filter in the presence of interference," in *Proceedings of the IEEE International Geoscience and Remote Sensing Symposium*, pp. 681–684, Cape Town, South Africa, July 2009.
[25] J. K. Hale and H. Kocak, *Dynamics and Bifurcation*, Springer-Verlag, Berlin, Germany, 1991.
[26] S. Wiggins, *Introduction to Applied Nonlinear Dynamical Systems and Chaos*, Springer-Verlag, Berlin, Germany, 1990.
[27] Y. Bar-Shalom, X. R. Li, and T. Kirubarajan, *Estimation with Application to Tracking and Navigation*, John Wiley, Hoboken, NJ, USA, 2001.